ARTICLE

Biosensor surface functionalization by a simple photochemical immobilization of antibodies: experimental characterization by mass spectrometry and surface enhanced Raman spectroscopy

Bartolomeo Della Ventura,[a] Marella De Angelis,[b] Martina Banchelli,[b] Paolo Matteini,[b] Riccardo Funari,[c†] Anna Illiano,[d] Paola Taroni,[a] Angela Amoresano[d] and Raffaele Velotta*[c]

Surface functionalization is a key step in biosensing since it is at the base of an effective analyte recognition. Among all the bioreceptors, antibodies (Abs) occupy a key role thanks to their superior specificity, although the available immobilization strategies suffer from several drawbacks. When gold is the interacting surface, the recently introduced Photochemical Immobilization Technique (PIT) has shown to be a quick, easy-to-use and very effective method to tether Abs oriented upright by means of thiols produced via tryptophan mediated disulphide bridge reduction. Although the molecular mechanism of this process is quite well identified, the detailed morphology of the immobilized antibodies is still elusive due to inherent difficulties related to the microscopy imaging of Abs. The combination of Mass Spectrometry, Surface-Enhanced Raman Spectroscopy and Ellman's assay demonstrates that Abs irradiated under the conditions in which PIT is realized, show only two effective disulphide bridges available for binding. They are located in the constant region of the immunoglobulin light chain so that the most likely position Ab assumes is side-on, i.e. with one Fab (i.e. the antigen binding portion of the antibody) exposed to the solution. This is not a limitation of the recognition efficiency in view of the intrinsic flexibility of the Ab structure, which makes the free Fab able to sway in the solution, a feature of great importance in many biosensing applications.

1. Introduction

Quantification of biological or biochemical processes are of utmost importance for medical, biological and biotechnological applications making biosensors development an attracting research field for its enormous potential impact in daily life.[1,2] Biosensors are analytical devices integrating a layer of biomolecules (bioreceptor) eligible for molecular recognition, and a signal transducer. Enzymes,[3,4] antibodies (Abs),[5,6] nucleic acids[7] and aptamers[8] are examples of bioreceptors widely used in biosensing although molecularly imprinted polymers (MIPs) are attracting noticeable interest for their larger stability.[9,10] MIPs are artificial receptors that mimic natural recognition biomolecules with a predetermined selectivity and specificity for a given analyte, thus they can be used as an ideal material in various applications, in particular for replacing the natural receptor molecules in biosensing.[11] Nevertheless, MIPs show several drawbacks in their quite complex synthesis (beads, membranes, *in situ* prepared monoliths) and in the subsequent surface imprinting[12] so that "natural" bioreceptors are still a standard in biosensor design. In this respect, in spite of some possible limitation, antibodies are prime candidates to be used for biorecognition as they are exquisitely designed and engineered to this aim.[13]

Immunoglobulins (Igs) or antibodies are highly soluble serum glycoproteins involved in the defense mechanisms of the immune system. They can be divided into five classes depending on their heavy chain constant region sequences, i.e. IgM, IgD, IgG, IgE and IgA.[14] A typical Ab is a large molecule (figure 1) with molecular weight of approximately 150 kDa made up of four polypeptide chains made of two heavy chains (red and cyan in panel b) of figure 1) and two light chains (κ in green and λ in yellow in panel b) of figure 1), which are joined together by disulfide bonds. The resulting tetramer has two identical halves, which together form the characteristic Y-like shape. The Fragment antigen binding (Fab) domain contains the complementarity-determining regions (CDRs), which constitute the antigen-binding sites of the Ab that provides the high antigen specificity.[15] Each end of the Y-shaped structure contains an identical antigen-binding site. The heavy chain is formed by one variable domain (variable heavy or V_H) and three constant domains (C_H1, C_H2, and C_H3). The light chain has one variable domain (variable light or V_L) and one constant domain (C_L).

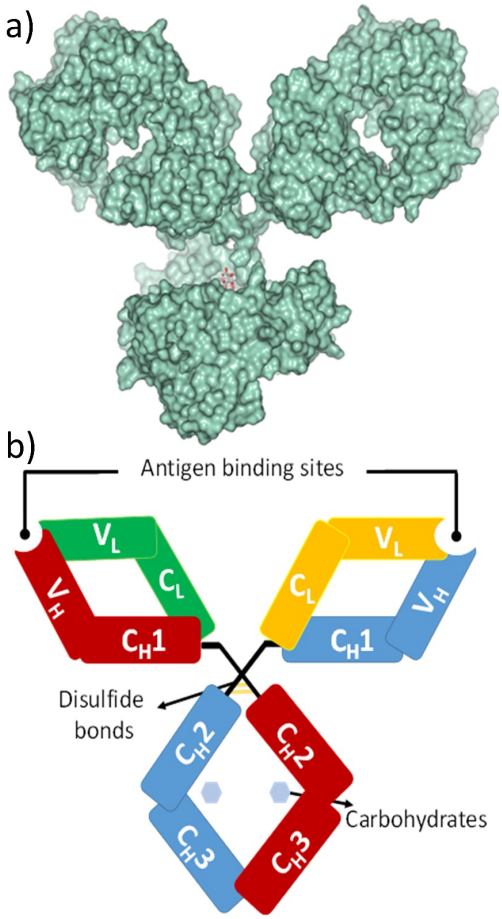

Figure 1 – (a) Spheres representation based on the X-ray crystallographic structure of 1IgY from protein databank. (b) Block scheme of an IgG.

The possible orientations an Ab can assume on a surface can be grouped in four categories (Figure 2):[5,16] tail-on and side-on, in which at least one Fab is free and exposed to antigens, as well as head-on and flat-on corresponding to both Fabs hidden and, hence, unavailable for antigen recognition. Since the orientation of Abs determine to a large extent the overall performances of the device,[17] the biosensor surface functionalization procedure is a crucial step in any protocol. Relying on electrostatic interactions (e.g. van der Waals or ionic forces), Abs can be easily tethered to a surface, but the resulting non-covalent bond has two main drawbacks in the relative weakness of the bond and, even more important, the random orientation of Abs. This last issue can be overcome resorting to intermediate proteins (e.g. protein A and protein G) that binds Fc region of the antibody so that tail-on orientation is favored, but such a non-covalent approach has an important disadvantage in the protein-antibody disassembling when the regeneration is carried out,[6] an issue made more acute by the length of the functionalization procedure. Moreover, possible involvement of the protein affinity domain in the interaction with the surface may even lead to sub-optimal immobilization.[18]

Stronger bonds can be achieved by surface modification with reactive groups such as hydroxy, thiol, carboxy or amino groups for the subsequent Ab covalent immobilization.[19] However, the chemistry involved in these processes is usually complex and time-consuming so that the whole production step turns out to be expensive.[20] Moreover, covalent conjugation of Abs onto solid surfaces using chemical linkers does not guarantee high antigen binding efficiency in view of the possible modification of the antigen binding sites as well as the lack of control on protein orientation.[21,22] Higher degree of orientation can be achieved by making photoactivatable the Fc region of the Ab, so that the latter can be site-selectively immobilized, but the whole strategy is quite complex and requires a previously prepared surface.[23] Site-specific immobilization technique based on UV activation of pristine IgGs (Photochemical Immobilization Technique, PIT) has been recently introduced,[24] and demonstrated to be effective in a number of circumstances with quartz-crystal microbalances (QCMs) for detecting small analytes[25,26] as well as large antigens.[24,27] Recently, PIT has been successfully applied also in detecting bacteria[28] and even extended to plasmonic sensors.[29,30] Such a surface functionalization technique is easy to apply, reproducible and cheap leading to a 10/20-fold enhancement antigen-binding detection compared to randomly immobilized Abs.[25,26] Despite of being routinely used to functionalize metal surfaces (gold) with high efficiency, only partial evidence of the whole mechanism underlying PIT has been reported.[31]

Photochemical Immobilization Technique is based on the selective photoreduction of the disulfide bridge in the cysteine–cysteine/tryptophan triads,[32] a typical structural feature of the IgG.[33] The UV-excitation of the tryptophan (trp) leads to the generation of solvated electrons, which are captured by the near disulfide bridge resulting in the destabilization and subsequent breakage of the cysteine–cysteine bond. The free thiol groups so produced interact with the metal surfaces in such a way that the subsequent functionalization enhances the antigen detection efficiency of the immunosensor.[24] The UV irradiation described here does not affect the intrinsic selectivity of the antibodies,[24–30] and can be considered an example of thiol-*click* photochemistry for surface functionalization in

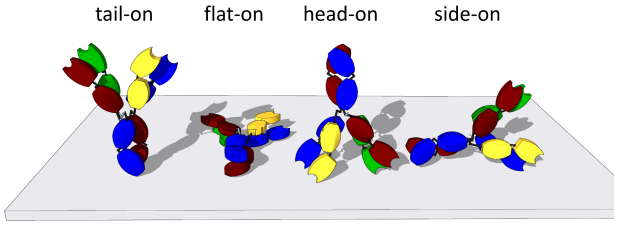

Figure 2 – Possible positions Ab can take up on the surface.

biosensing.[34] However, although there is already a clear evidence that UV light is able to orient antibodies onto the substrates, there is still a lack of direct demonstration of which triad of aminoacids is directly responsible of the protein immobilization upon the activation by UV-light.

In this manuscript, we provide a detailed microscopic characterization of PIT by identifying the functional groups responsible for the covalent bonding of Ab to a metal surface by means of mass spectrometry, Surface-Enhanced Raman Spectroscopy (SERS) and biochemical tools such as Ellman's assay. In particular, we show that appropriate UV irradiation of IgG leads to the formation of mostly four SH groups, two of them available for Ab immobilization, thereby offering a molecular description of PIT mechanism. We demonstrate that by irradiating Abs in solution for only 30 s with UV light from an amalgam type lamp (≈1 W/cm^2 on the sample), we are able to produce "activated Abs" with approximately 8 reduced thiols (≈4 disulphide bridge open per Ab). Once opened, the thiol residues keep their properties for at least 200 s, a time long enough to convey Abs onto a metal (gold or silver) surface on which they bind upright. The position of free cysteines has been determined by mass spectrometry, which also confirms that only 8 thiols per Ab are reduced by UV and 4 of them (i.e. 2 disulphide bridges) are not exposed to the solvent lowering to two the number of bridges available for PIT. Moreover, SERS highlights that the signal from UV-treated Abs is much stronger than that coming from Abs physisorbed, thereby demonstrating higher proximity of Abs with the surface when they are UV-activated.

2. Experimental section

2.1. UV irradiation of immunoglobulins

We realized the PIT by irradiating a solution of 50 µg/mL of immunoglobulins type G (IgG) for 30 s with a HERAEUS amalgam type NNI 40/20 lamp emitting at 258 nm with a power of 40 W. The intensity of the lamp used in this experiment was about 0.7 W/cm^2 very close to the surface. By considering that the quartz cuvette containing the IgG solution was located at 1 cm from the lamp surface, the effective irradiation intensity used for the antibody activation was about 0.5 W/cm^2.

2.2. Mass spectrometry

All reagents were purchased from Sigma Aldrich, Milan, Italy. Two different IgG standard proteins (30 and 50 µg) were exposed to UV radiation (λ=258 nm) for three different time point: 30 s, 60 s, 90 s. Irradiated IgG standard proteins were treated with 50 mM iodoacetamide 1:5 molar excess compared to the number of cysteine to block the disulfide bonds reduced by irradiation. The reaction was carried out at room temperature for 30 min in the dark. The solution was subjected to methanol, chloroform, water precipitation protocol and the protein pellet recovered was dried under vacuum.

Reduction of disulfide bonds was performed by using 10 mM dithiothreitol in 1:10 molar excess compared to the number of moles of cysteine residues present in the protein in denaturing buffer (6M Guanidine, Trizma 300 mM, EDTA 10 mM, pH 8). Reaction was performed for 2 h at 37 °C.

Proteins were precipitated with methanol, chloroform and water protocol and the recovered protein pellet was subjected to tryptic digestion using an amount of enzyme in a ratio of 1:50 with the amount of protein. The peptide mixture was sub digested with chymotrypsin in a 1:20 ratio with the amount of processed protein. Enzymatic digestions were carried out for 18 h at 37 °C. Peptide mixture was analyzed by MALDI TOF. Matrix-assisted laser desorption/ionization (MALDI) mass spectrometry (MS) experiments were performed on a 4800 MALDI-TOF-TOF ABSciex equipped with a nitrogen laser (337 nm). Calibration was performed by using AB SCIEX calibration mixture (Monoisotopic (M+ nH)n+: 904.46 Da des-Arg-Bradykinin, 1296.68 Da Angiotensin I, 1570.67 Da Glu-Fibrinopeptide B, 2093.08 Da ACTH (clip 1–17), 2465.19 Da ACTH (clip 18–39), 3657.92 Da ACTH (clip 7–38)). 0. 5 µL of the sample (1/1, v/v) was mixed with a 10 mg/mL solution of α-cyano-4-hydroxycinnamic acid in 70:30 acetonitrile:50 mM citric acid in water solution. Spectra were acquired using a mass (m/z) range of 300–3000 Da for peptide identification.

2.3. Fabrication of the AgNC-Chip

AgNCs were deposited onto a gold-coated QCM chip by slightly modifying a previous protocol.[35,36] Briefly, n-hexane (0.4 mL) was placed at the bottom of a PTFE cell (5 cm^2 area) and 0.08 mL of an aqueous nanocube suspension was added afterwards. 0.16 mL of EtOH was then dropped at the top of the hexane phase, leading to the assembly of nanoparticles at the water–hexane interface. The floating nanoparticles firmly adhered to the QCM crystal upon complete solvent evaporation. The substrates were finally washed twice with water and ethanol and, after overnight drying, were subjected to a 10 min plasma treatment (ZeptoDiener Plasma Surface Technology operating at 40 kHz and 1 mbar air) before use.

2.4. Immobilization of IgG on the AgNC-chip and QCM protocol

The fluidic circuit consists of a cell containing the oscillator, tygon tubes, reservoir for the solution and the pump.[24] When needed aliquots of 0.5 mL solution of the antibody into milliQ water are irradiated by UV light and quickly transferred to the fluidic reservoir. The relation between the frequency variation of the balance and the mass deposition Δm is given by the Sauerbrey equation[37] from which we have $\Delta f = -K(\Delta m)$, K being a constant depending on several experimental parameters (resonance frequency, crystal active area, quartz density and shear modulus for AT-cut crystal). The experimental protocol for IgG immobilization included the following steps: (1) measurement of the oscillator frequency in air for the AgNC-chip, which is compared with that of a undecorated chip as reference to estimate the mass of deposited metal; (2) mounting of the AgNC-chip into the fluidic circuit followed by cleaning with milliQ water, which also allows to reach the

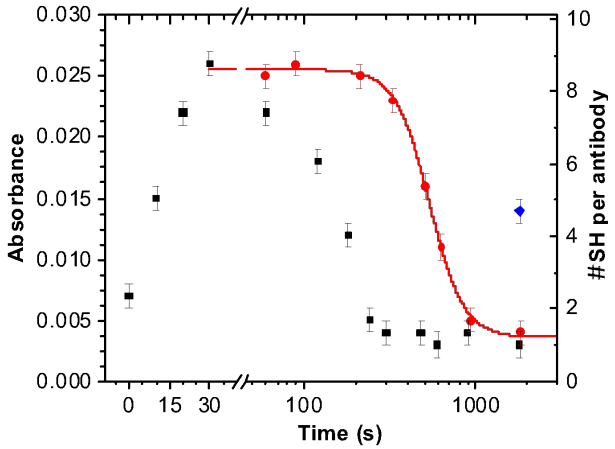

Figure 3. TNB^{2-} absorbance (Ellman's assay) and number of free thiols per Ab as a function of irradiation time. The Ab concentration is 25 μg/mL. The black square points refer to thiols yielded immediately after irradiation and show an optimum irradiation time of 30 s. A sample irradiated for 30 s has been tested by adding the Ellman reagent after different "waiting time" and the results (red circle points) show that for approximately 300 s no significant change occurs in the thiol concentration. After a waiting time of 1800 s the solution was re-irradiated for 30 s and the thiol concentration soon after the irradiation recovered by approximately 50% (blue diamond point).

basal frequency stabilization; (3) circulation of the antibody solution; (4) final washing step with milliQ water to eliminate weakly bonded material. Three replicates of three chips have been prepared as described: one without antibodies contained in the buffer solution of the fluidic circuit, which is used as reference, and the other two exposed to untreated and UV-activated antibodies.

2.5. Raman Spectroscopy

Raman spectroscopy was carried out under a microRaman Horiba Xplora system coupled to a 532 nm diode laser. Single acquisitions of 10 sec with a laser power at the sample of ~2 mW and a diffraction grating of 1200 l/mm were performed. The backscattered signal was acquired by focusing the laser beam on the nanoparticle layer by means of a 10X microscope objective (0.25 NA), generating a ~7μm size beam waist that provides an average response in turn minimizing possible local signal variability. The spectra represent the average of 50 random measurement points from 3 replicates. The Raman spectrum of a drop-casted (5 μL) aqueous solution of antibody on a gold mirror substrate was used as reference for mode assignment. Spectra were baseline subtracted when needed.

2.5. Reagents for Ellman's assay

5,5-dithio-bis-2-nitrobenzoate (DTNB, purity 99%) was purchased from Sigma–Aldrich and the "phosphate buffer/6 mM DTNB" mentioned throughout the paper contained 0.1 M phosphate buffer, pH 7.4, and 6 mM of DTNB.

3. Results and discussion

3.1. Ellman's assay

The occurrence of disulphide bridge(s) breaking has been quantified by the so-called Ellman's assay, based on a reagent [5,5'-dithiobis-(2-nitrobenzoic acid) or DTNB] used to quantify the concentration of thiol groups in a sample.[38] The reaction of a thiol with DTNB gives mixed disulfide and 2-nitro-5-thiobenzoic acid (TNB) as products. The thiol concentration is quantified by measuring the absorbance at 412 nm (relative to the anion TNB^{2-}) after the calibration of the assay (see Supplementary Information for details on the calibration). Figure 3 reports the absorbance and the UV-reduced disulphide bridges as a function of the irradiation time for a solution of Abs at 25 μg/mL. The absorbance reaches a maximum after 30 s irradiation, corresponding to approximately 4 disulfide bridges per Ab.

The occurrence of an optimum irradiation time (Figure 3 black points) is explainable by considering on the one hand the reduction induced by the UV light, which increases the number of free thiols with the time, and secondly the denaturation of the Abs, which takes place at long exposure time to UV radiation (i.e., high dose of absorbed light). The behavior of the UV-reduced disulphide bridges after different times before adding Ellman's reagent is also shown (Figure 3 red points). It is worth highlighting that the disulphide bridges remain open for 5 minutes, which can be considered the time available to bind the gold surface. The degree of reversibility of the process induced by the PIT has been tested by irradiating antibodies a second time after 30 minutes, a time long enough for the absorbance to return to the value measured with the initial solution (figure 3). The subsequent absorbance is 0.014 (blue diamond point in figure 3), which is approximately 50% of the maximum value obtainable for a fresh solution. Such a high recovery demonstrates that UV irradiation carried out in the conditions required for PIT does not induce significant denaturation processes.

3.2 Mass spectrometry

Among all analytical methods used to characterize monoclonal antibodies, mass spectrometry plays an increasingly important role for both global and fine structural characterization of the structures. We will discuss and will provide detailed protocols for antibody structure characterization to better investigate which cysteine, involved in disulphide bridges, are sensitive to UV irradiation and "hot spots" mapping. Interestingly, with the last generation of LC-ES-TOF mass spectrometers, the mass of intact antibodies can be measured with a precision reaching 40 ppm, which speeds-up considerably the screening and routine monoclonal antibodies identification. Peptide mass fingerprinting (PMF) performed by using liquid chromatography–mass spectrometry (LC-MS) is nowadays the standard analytical method for protein mapping. PMF is generally performed by comparing mass values detected in the chromatograms of peptides after enzymatic digestion with theoretical values. However, this method suffers some limits,

namely it is time-consuming and laborious due to long gradient time needed for HPLC separation and the extensive search to find a characteristic mass shift.[39] Thus, alternative strategies have been exploited. In this context, MALDI-TOF MS analyses combined with reflectron tools is a widely adopted technology used in proteomics.[40–42] This technique provides promising qualitative results resulting in the preferred solution for protein mapping because it offers a unique speed advantage over LC-MS in terms of greatly reduced instrument time and high accuracy and resolution.

Moreover, the current resolution of mass spectra allows also investigating the non-symmetry of N-linked biantennary oligosaccharides between the two heavy chains. This analysis was not feasible up to now with classical carbohydrate analytical methods used after enzymatic glycans release. These new types of information may contribute to the better knowledge of Fc gamma receptor binding structure relationships. On the other hand, MALDI-TOF mass measurements are less accurate for the intact antibody (2 heavy and 2 light chain), but gives direct information on the light chain mass and fragments. After disulfide bridge reduction, very acute data can be recorded for both light (25 kDa range) and heavy chains (50 kDa range). In addition, the efficacy of mass spectrometry over classical electrophoresis and liquid-chromatography methods has also recently demonstrated for posttranslational modifications that were not previously reported for monoclonal antibodies.

Chain	Cysteines position	Cysteines yield (UV irradiation)	Cysteines yield (control)	Domain
IGKC	C26 intrachain	25%	<5%	C_L
	C86 intrachain	15%	<5%	C_L
	C106 interchain	15%	15 %	Hinge region
IGH1M	C357 intrachain	15%	<5%	C_H3
	C302 intrachain	10%	<5%	C_H3
	C102 interchain	15%	15 %	Hinge region

Table 1. Cysteines with high yield (≥5%) identified by mass spectrometry after the UV irradiation carried out in the same conditions PIT is realized (amalgam lamp emitting at 254 nm with an intensity on the sample of ≈1 W/cm^2 for 30 s). C102 and C106 are detected also in the control and their presence may well account for the non-zero intercept in Figure 3. On the contrary, the occurrence of C26-C86 and C302-C357 is a result of the UV irradiation.

As a case study, we choose the monoclonal antibody anti-phenobarbital from host musculus since its sequence is well-known (Figure S1) and its crystallographic structure is available in the protein database.[43] The results (Figure S2) are reported in Table 1 that contains a comparison between the cysteines yield detected in irradiated and non-irradiated Ab. By considering a yield threshold of 5%, we found that the cysteines reduced by UV lamp are exclusively placed in the positions 26, 86, 106, 357, 302 and 102. Cysteines found in position 102 and 106 are also present in the control sample[44] and as such they can be discarded as the possible candidates for covalent Ab anchoring. From the analysis of the 3D structure of our Ab, it turns out that the four remaining cysteines (26-86 and 302-357) interact each other to form the disulfide bridges, which realizes the Cys-Cys-Trp triad. These disulfide bridges are localized in the light chain constant region (26-86) and in the heavy chain constant region (302-357), respectively. Since the antibodies are composed by two identical heavy and light chains, the mass spectrometry shows that UV irradiation (in the conditions required by PIT) leads to the reduction of only four disulfide bridges, a value in excellent agreement with the result obtained by the Ellman assay. While cysteines 302-357 are not exposed to the solvent,[45,46] and as such it is unlikely they contribute to bind the Ab to a surface, the cysteines 26-86 are located on the external surface of the antibody and, hence, they may well be the only candidate for PIT.

The protein concentrations we have used were 30 μg/mL, 50 μg/mL and 70 μg/mL with irradiation times of 30 s, 60 s and 90 s. The data reported in Figure 3 refer to solution 30 μg/mL of Abs irradiated for 30 s. We point out the occurrence of a drastic drop of the sequence coverage (only 25%) at each concentration when the irradiation time was 90 s. On the opposite, a high sequence coverage of 75% was found with an irradiation time of 30 s and 60 s for each of the three concentrations, exception made for 70 μg/mL and 60 s irradiation time that showed again a low sequence coverage. We ascribe such a behavior to the denaturation of the Abs induced by UV irradiation, but also to the aggregation promoted by the presence of the produced SH radicals. The formation rate of the aggregates is linearly dependent on the initial Ab concentration, but it is expected to be dependent more than linearly on the irradiation time, which also enters into the activation process. Thus, both Ellman's assay and the mass spectrometry analysis suggest that the optimal irradiation time is approximately 30 s and the initial Ab concentration should never exceed 50 μg/mL.

3.3. SERS (Surface Enhanced Raman Scattering)

The UV light-induced anchoring of IgGs to 50 nm-size silver nanoparticles with a cubic shape (silver nanocubes, AgNCs) was monitored by QCM analysis. We note that these nanoparticles represent a convenient choice for studying bio-nano interactions due to the availability of solid synthesis protocols ensuring well-defined geometrical and optical

properties[47] (Figure S3). In particular they show quasi single-crystal features with dominating low-energy (100) facets,[48] which largely simplify the surface chemistry guiding the protein immobilization.[49,50] Nonetheless, the application of plasmonic nanoparticles with non-spherical geometry is attracting growing interest in biosensing[51] and in other biodetection schemes[36,52]due to their amplifying antenna-like behavior.

QCM measurements was useful to monitor and optimize the antibody immobilization by tracking mass differences when the antibodies are tethered on the nanoparticle surface. IgG immobilization was performed on AgNCs-deposited gold-coated QCM chips (referred as AgNCs@QCMChips in the following) by using a microfluidic system designed to have a controlled flux of untreated or UV-treated IgG solutions onto the plasmonic surface (see Experimental Section for details). A Raman investigation was performed to gain detailed insights into the local anchoring geometry of the IgG layer formed on the surface of the metal nanostructures. Here AgNCs act as effective nanoantennas to dramatically enhance the Raman signal of chemically or physically adsorbed IgG in turn allowing the collection of its vibrational spectrum in spite of a low local protein density. Thus the samples were analysed by microRaman spectroscopy and their surface-enhanced Raman (SER) spectra (Figure 4) were compared to the Raman signal of a dried deposit of the antibody (Figure S4). A nice matching between SER and Raman spectra let us identify the main vibrational modes of IgG as detailed in Table S1. We observed a high point-to-point reproducibility with intensity values depending on the amount of anchored antibody. Therefore, SER spectra were normalized considering the frequency shift obtained with the QCM measurements. A 1.5-fold increase of the band centered at 240 cm^{-1}, including modes associated with the Ag-S stretching, immediately emerges from comparing UV-treated with untreated sample (Figure S5a, Table S2). We can infer that upon light-induced breaking of disulfide bridges in the protein, a larger number of free thiol groups are available for bonding with the metal surface[53]. A comparable increase in the 653 cm-1 mode (Figure S5b) supports a larger amount of C-S bonds proximal to the Ag surface, which is in line with the formation of Ag-S bonds once Cys residues are activated by UV radiation[54].

The specific involvement of the C26/C86 pair governing the UV-induced IgG immobilization is supported by considering the Raman modes associated with its aromatic residues. These typically display prominent signals in the Raman spectra of proteins that are extremely susceptible to plasmonic enhancement. Accordingly, Phe (F), Tyr (Y) and Trp (W) spectral signals appear ≈3-fold more intense in the spectrum of the UV-treated sample (Figure S5c and d, Table S3). Specifically, an increase in the bands characteristic of Phe, namely 1003, 1031, 1205, 1603 cm^{-1}, is well justified by a closer proximity of F27 and F31 to C26 (see Figure 4) residue covalently bonded to the plasmonic surface. In a similar fashion, increased Trp modes at 756, 877, 1330 and 1555 cm-1 and Tyr modes at 830, 850 and 1612 cm^{-1} can be assigned to

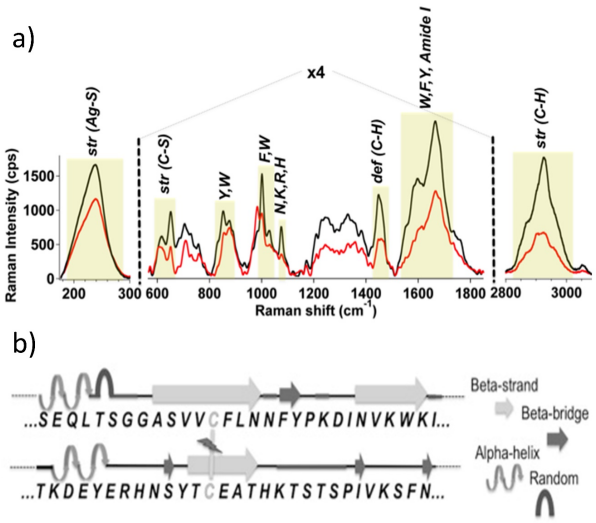

Figure 4. a) Recap of representative SER spectral regions of UV-activated (black) and nonactivated (red) samples. Signals within the 600-1800 cm-1 region were 4x multiplied for clarity. b) Sequence of aminoacids and secondary structures comprising the interchain bridge between C26 and C86 cysteine residues involved in the UV-activation.

W40 and Y32,Y84 residues respectively, which, being contiguous to C26 and C86 (Figure S6), are forced to adopt an outer positioning as a result of the antibody anchoring. Interestingly, the relative intensity of the 830 and 850 cm^{-1} doublet of Tyr appears different when moving from the unirradiated to the irradiated sample. The relative intensities of the two bands are a common marker used for tertiary structure prediction because depends on the presence of a hydrogen-bonded phenyl ring of the lateral chain[54]. Thus a higher band ratio as observed in the UV-treated sample may indicate a higher exposure of Tyr residues to the aqueous environment as a consequence of the formation of Cys/metal bonds.

The evidence that the UV-immobilized protein is higher strong-bonded to the silver nanochip arises from the analysis of those spectral regions characteristic of its conformation and secondary structure. Noteworthy, important spectral changes occur in the conformationally sensitive region of the protein skeletal modes involving C-C and C-N stretching vibrations (900-1130 cm^{-1}). Despite a significant decrease in the intensity of the band between 980 and 990 cm^{-1} (assigned to the Amide III antiparallel b-sheet mode), in the UV-treated sample a marked increase (around 5-fold) is displayed in the band centered at 1076 cm^{-1}, accounting for the C-N bonds of the backbone chain. This is rightfully consistent with a very close vicinity of IgG polypeptidic chain to the AgNChip, at a great major extent respect to the untreated protein.

Additionally, the spectral region at 1500-1800 cm^{-1} also shows much higher intensities of the UV treated sample. In this region Amide I and few bands of the *AA*Trp and Phe are also

present. These bands, together with the secondary structure of a helices, random coils and b-sheet can be resolved with a multipeak fit procedure (see Supplementary Information). From these analysis we can say that the overall contribution due to the Amide I secondary structure is highly increased in the UV-treated sample, together with the signal from the random coil structures that are the most in the antibody under study.

The spectral region between 2800-3000 cm^{-1} is characteristic for the presence of the stretching vibrations of the C-H bonds of the CH_2 and CH_3 groups. These groups are placed along the whole polipeptidic chain. We can observe that for these bands the signal in the UV treated sample is higher than in the not treated one and this trend is also confirmed by the increased band intensity in the 1420-1480 region. We can infer that in the case of the UV treated antibodies more aliphatic or methylated amino acids, such as A, V, T, N, are closer to the metal surface respect to the UV un-treated proteins. This proximity cannot derive from a chemical (electrostatic or van der Waals) attraction, but rather from an approach contrived by the new UV induced Ag-S bond.

3.4. Modeling IgG morphology resulting from PIT

Two independent characterizations (mass spectrometry and Ellman's assay) demonstrate that only 4 disulfide bridges (C26-C86 and C302-C357), among the twelve potentially involved in the process, are reduced by UV irradiation carried out in the same conditions required for PIT. The photochemical reduction only occurs for one of the cystines located in the constant region of the light chain (C26-C86) and for one located in the constant region of the heavy chain (C302-C357) with a yield higher for the former. To shed light on the mechanisms underlying such a selective process, we analysed the IgG structure with Protein Imager 2.0[55] finding that most of the twelve triads are very close to phenylalanine and tyrosine, the other aromatic aminoacids that absorb UV light (Figure 5a). Indeed, only two triads are completely free and far from tyrosine and phenylalanine (Figure 5b) and they correspond to C26-C86. The remaining cysteines are fully surrounded by the other aromatic aminoacids, exception made for C302-C357 that are surrounded by the only phenylalanine and, hence, are able to be photo-chemically reduced although at lower rate as it turns out from mass spectrometry measurements. On the other hand, the slightly screened bridge C302-C357 is not well exposed to the solvent,[45,46] and as such it is unable to bind the surface. Thus, the selectivity of the UV irradiation under PIT conditions can be ascribed either to the screen role played by tyrosine and phenylalanine, which hampers the bridge reduction, or to a poor exposition to the solvent as it is the case for C302-C357. Thus, the UV-treated antibodies can anchor themselves onto the surfaces only through reduced cysteines C26 and C86.

We can gain insight of the morphological behaviour of the IgGs when immobilized onto a planar surface by considering the flexibility and dynamics these proteins have in solution as determined by analysing their AFM and SAXS images.[56,57] It has been shown that the distribution of the angle ϑ between the two Fab domains (Figure 6a) when the antibodies are in a solution, is quite peaked around 120°. On the opposite, the distribution of the angle between the normals to the domain planes is almost uniform in the range 10° to 90°. These results demonstrate the high flexibility of the Ab conformation also suggesting that the flat-on position (Figure 2) is quite unlikely.[56] Since our analysis suggests the immobilization by the thiol produced in the variable part of the light chain, we conclude that PIT makes more likely the side-on position as reproduced in Figure 6b. Given the high flexibility shown by Abs, if one Fab domain is bound to the surface, the other experiences all the possible conformation allowed by $10° < \varphi < 90°$. Such a result confirms the consistency of the hypothesis about the Ab orientation induced by PIT previously proposed.[31] Moreover, it justifies the effectiveness of such a functionalization strategy since it leads to strong (covalent) bond of Ab to the surface while orienting it side-on with one Fab exposed to the solution (Figure 6b).

4. Conclusions

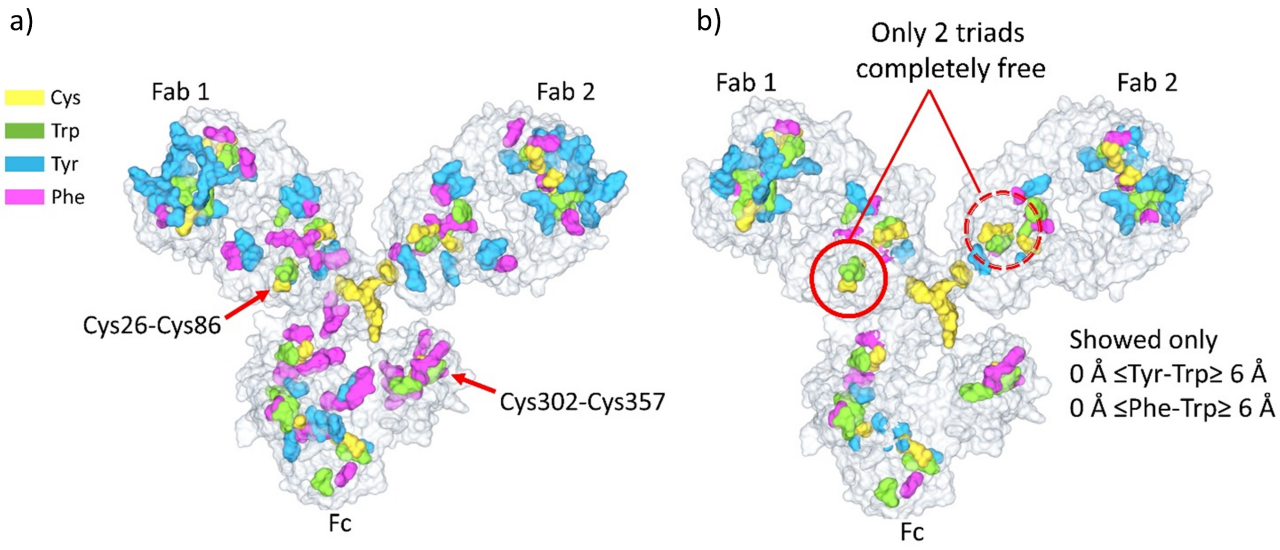

Figure 5. 3D structure of IgG 1IgY taken from Protein Data Bank (PDB) showing (a) all the aromatic aminoacids and cysteines. In (b) the same picture is reported with aromatic aminoacids whose distance from triad is smaller than 6Å.

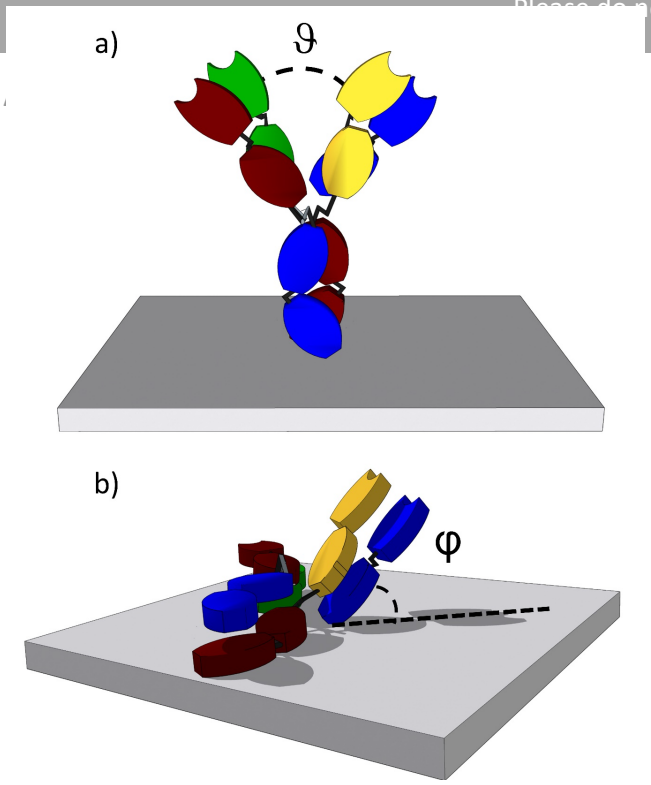

Figure 6. a) The angle ϑ between the two Fabs has a distribution peaked at approximately 120°. b) IgG onto the surface in the position expected when PIT is realized. The angle ϕ spans almost uniformly the range 10° to 90° thereby providing one Fab well-exposed to the solvent.

Our work has demonstrated the effectiveness of PIT in the selective breaking of the disulfide bridges in IgG antibody, thereby producing highly reactive free thiols. These allow the right orientation of the Ab Fab region once the Ab is immobilized onto metal surfaces. As a consequence, this technique offers a powerful tool to drive the antibody immobilization thus resulting in a significant increase in the number of effective antigen binding sites available onto any metal transducer. The presented one-step photochemical functionalization method opens interesting perspectives in the sensor research since a wide range of highly sensitive and specific biosensing technologies employing Abs as biorecognition elements (e.g. antibody microarray devices[58]) would take advantage of it, thus greatly enhancing their performances. PIT is brilliantly competitive against alternative methods to anchor proteins onto metal surfaces, since it prevents the use of expensive toxic chemical reagents which require long and complex chemical procedures in well-equipped laboratories. On the contrary, PIT can be safely run by non-expert personnel, it is rapid and user-friendly.
Measurements carried out by mass spectrometry, SERS and Ellman's assay in the present work allowed to identify the reduced cysteines produced by PIT and to unequivocally highlight the process behind PIT irradiation. Moreover, knowing the exact location of the reactive disulphide bridges, it has been possible to simulate the position and the different conformations that IgGs can assume on planar surfaces after covalent PIT-induced anchoring.

Conflicts of interest

There are no conflicts to declare.

Acknowledgements

P.M., M. de A. and M.B. acknowledge financial support from the Tuscany Region in the framework of the PAR FAS 2007-2013 Action Line 1.1- Action 1.1.2 SUPREMAL project.

References

1 G. Rong, S. R. Corrie and H. A. Clark, *ACS Sensors*, 2017, **2**, 327–338.
2 Z. Farka, T. Juřík, D. Kovář, L. Trnková and P. Skládal, *Chem. Rev.*, 2017, **117**, 9973–10042.
3 S. M. Borisov and O. S. Wolfbeis, *Chem. Rev.*, 2008, **108**, 423–461.
4 D. Grieshaber, R. MacKenzie, J. Vörös and E. Reimhult, *Sensors*, 2008, **8**, 1400–1458.
5 A. K. Trilling, J. Beekwilder and H. Zuilhof, *Analyst*, 2013, **138**, 1619–27.
6 A. Makaraviciute and A. Ramanaviciene, *Biosens. Bioelectron.*, 2013, **50**, 460–471.
7 Y. Du and S. Dong, *Anal. Chem.*, 2017, **89**, 189–215.
8 N. Aliakbarinodehi, P. Jolly, N. Bhalla, A. Miodek, G. De Micheli, P. Estrela and S. Carrara, *Sci. Rep.*, 2017, **7**, 44409.
9 A. Poma, A. P. F. Turner and S. A. Piletsky, *Trends Biotechnol.*, 2010, **28**, 629–637.
10 L. Uzun and A. P. F. Turner, *Biosens. Bioelectron.*, 2016, **76**, 131–144.
11 K. Mosbach and O. Ramström, *Nat. Biotechnol.*, 1996, **14**, 163–170.
12 E. V Piletska, R. Guerreiro, M. J. Whitcombe and S. A. Piletsky, 2009, 4921–4928.
13 S. K. Vashist and J. H. T. Luong, in *Handbook of Immunoassay Technologies*, Elsevier, Weinheim, Germany, 2018, vol. 3–4, pp. 1–18.
14 C. A. Janeway, Jr., P. Travers, M. Walport and M. J. Shlomchik, *Immunobiology*, Garland Science, New York, 5th edn., 2001.
15 P. J. Conroy, S. Hearty, P. Leonard and R. J. O'Kennedy, *Semin. Cell Dev. Biol.*, 2009, 20, 10–26.
16 S. Sharma, H. Byrne and R. J. O'Kennedy, *Essays Biochem.*, 2016, **60**, 9–18.
17 A. K. Trilling, M. M. Harmsen, V. J. B. Ruigrok, H. Zuilhof and J. Beekwilder, *Biosens. Bioelectron.*, 2013, **40**, 219–26.
18 M. Shen, J. F. Rusling and C. K. Dixit, *Methods*, 2017, **116**, 95–111.
19 L. S. Wong, F. Khan and J. Micklefield, *Chem. Rev.*, 2009, **109**, 4025–4053.
20 N. G. Welch, J. A. Scoble, B. W. Muir and P. J. Pigram, *Biointerphases*, 2017, **12**, 02D301.
21 Y. Jung, J. Y. Jeong and B. H. Chung, *Analyst*, 2008, **133**, 697–701.
22 S. K. Vashist, C. K. Dixit, B. D. MacCraith and R. O'Kennedy,

Analyst, 2011, **136**, 4431–4436.
23 Y. Lee, J. Jeong, G. Lee, J. H. Moon and M. K. Lee, *Anal. Chem.*, 2016, **88**, 9503–9509.
24 B. Della Ventura, L. Schiavo, C. Altucci, R. Esposito and R. Velotta, *Biomed. Opt. Express*, 2011, **2**, 3223–3231.
25 R. Funari, B. Della Ventura, L. Schiavo, R. Esposito, C. Altucci and R. Velotta, *Anal. Chem.*, 2013, **85**, 6392–7.
26 R. Funari, B. Della Ventura, R. Carrieri, L. Morra, E. Lahoz, F. Gesuele, C. Altucci and R. Velotta, *Biosens. Bioelectron.*, 2015, **67**, 224–229.
27 B. Della Ventura, N. Sakač, R. Funari and R. Velotta, *Talanta*, 2017, **174**, 52–58.
28 A. Fulgione, M. Cimafonte, B. Della Ventura, M. Iannaccone, C. Ambrosino, F. Capuano, Y. T. R. Proroga, R. Velotta and R. Capparelli, *Sci. Rep.*, 2018, **8**, 16137.
29 M. Iarossi, C. Schiattarella, I. Rea, L. De Stefano, R. Fittipaldi, A. Vecchione, R. Velotta and B. Della Ventura, *ACS Omega*, 2018, **3**, 3805–3812.
30 B. Della Ventura, M. Gelzo, E. Battista, A. Alabastri, A. Schirato, G. Castaldo, G. Corso, F. Gentile and R. Velotta, *ACS Appl. Mater. Interfaces*, 2019, **11**, 3753–3762.
31 R. Funari, B. Della Ventura, C. Altucci, A. Offenhäusser, D. Mayer and R. Velotta, *Langmuir*, 2016, **32**, 8084–8091.
32 M. T. Neves-Petersen, Z. Gryczynski, J. Lakowicz, P. Fojan, S. Pedersen, E. Petersen and S. Bjørn Petersen, *Protein Sci.*, 2002, **11**, 588–600.
33 T. R. Ioerger, C. Du and D. S. Linthicum, *Mol. Immunol.*, 1999, **36**, 373–386.
34 M.-J. Bañuls, M. Á. González-Martínez, J. Sabek, J. García-Rupérez and Á. Maquieira, *Anal. Chim. Acta*, 2019.
35 F. Reincke, S. G. Hickey, W. K. Kegel and D. Vanmaekelbergh, *Angew. Chemie Int. Ed.*, 2004, **43**, 458–462.
36 P. Matteini, M. De Angelis, L. Ulivi, S. Centi and R. Pini, *Nanoscale*, 2015, **7**, 3474–3480.
37 G. Sauerbrey, *Zeitschrift für Phys.*, 1959, **155**, 206–222.
38 G. L. Ellman, *Arch. Biochem. Biophys.*, 1959, **82**, 70–77.
39 L. Dai, R. Preston, M. Bacica, A. Kinhikar, B. Bolaños and R. E. Murphy, *Bioconjug. Chem.*, 2013, **24**, 53–62.
40 W. Pusch and M. Kostrzewa, *Curr. Pharm. Des.*, 2005, **11**, 2577–2591.
41 A. Amoresano, A. Carpentieri, C. Giangrande, A. Palmese, G. Chiappetta, G. Marino and P. Pucci, *Clin. Chem. Lab. Med.*, 2009, **47**, 647–65.
42 Y. Yefremova, M. Al-Majdoub, K. F. M. Opuni, C. Koy, W. Cui, Y. Yan, M. L. Gross and M. O. Glocker, *J. Am. Soc. Mass Spectrom.*, 2015, **26**, 482–492.
43 L. J. Harris, E. Skaletsky and A. McPherson, *J. Mol. Biol.*, 1998, **275**, 861–872.
44 N. M. Gevondyan, A. M. Volynskaia and V. S. Gevondyan, *Biochem.*, 2006, **71**, 279–284.
45 L. M. Amzel and R. J. Poljak, *Annu. Rev. Biochem.*, 1979, **48**, 961–997.
46 H. Kikuchi, Y. Goto and K. Hamaguchi, *Biochemistry*, 1986, **25**, 2009–2013.
47 M. Banchelli, B. Tiribilli, M. De Angelis, R. Pini, G. Caminati and P. Matteini, *ACS Appl. Mater. Interfaces*, 2016, **8**, 2628–2634.
48 M. Rycenga, X. Xia, C. H. Moran, F. Zhou, D. Qin, Z. Y. Li and Y. Xia, *Angew. Chemie - Int. Ed.*, 2011, **50**, 5473–5477.
49 J. Feng, J. M. Slocik, M. Sarikaya, R. R. Naik, B. L. Farmer and H. Heinz, *Small*, 2012, **8**, 1049–1059.
50 F. Tavanti, A. Pedone, P. Matteini and M. C. Menziani, *J. Phys. Chem. B*, 2017, **121**, 9532–9540.
51 L. Guo, J. A. Jackman, H. H. Yang, P. Chen, N. J. Cho and D. H. Kim, *Nano Today*, 2015, **10**, 213–239.
52 P. Matteini, M. Cottat, F. Tavanti, E. Panfilova, M. Scuderi, G. Nicotra, M. C. Menziani, N. Khlebtsov, M. De Angelis and R. Pini, *ACS Nano*, 2017, **11**, 918–926.
53 I. Martina, R. Wiesinger and M. Schreiner, *e-Preservation Sci.*, 2012, **9**, 1–8.
54 E. Podstawka, Y. Ozaki and L. M. Proniewicz, *Appl. Spectrosc.*, 2004, **58**, 1147–1156.
55 G. Tomasello, *Protein Imager 2.0. Retrieved from https//3dproteinimaging.com/*.
56 X. Zhang, L. Zhang, H. Tong, B. Peng, M. J. Rames, S. Zhang and G. Ren, *Sci. Rep.*, 2015, **5**, 9803.
57 Q. Chen, M. Vieth, D. E. Timm, C. Humblet, D. Schneidman-Duhovny, I. E. Chemmama, A. Sali, W. Zeng, J. Lu and L. Liu, *PLoS One*, 2017, **12**, e0175758.
58 D. B. Bush and T. A. Knotts, *J. Chem. Phys.*, 2018, **149**, 165102.